Low-order continuous finite element spaces on hybrid non-conforming hexahedral-tetrahedral meshes

Maxence Reberol, Bruno Lévy

HAL Id: hal-01313285

https://hal.archives-ouvertes.fr/hal-01313285

Submitted on 9 May 2016

Low-order continuous finite element spaces on hybrid non-conforming hexahedral-tetrahedral meshes

Maxence Reberol, Bruno Lévy

INRIA Nancy Grand-Est

Abstract

This article deals with solving partial differential equations with the finite element method on hybrid non-conforming hexahedral-tetrahedral meshes. By non-conforming, we mean that a quadrangular face of a hexahedron can be connected to two triangular faces of tetrahedra. We introduce a set of low-order continuous (C^0) finite element spaces defined on these meshes. They are built from standard tri-linear and quadratic Lagrange finite elements with an extra set of constraints at non-conforming hexahedra-tetrahedra junctions to recover continuity. We consider both the continuity of the geometry and the continuity of the function basis as follows: the continuity of the geometry is achieved by using quadratic mappings for tetrahedra connected to tri-affine hexahedra and the continuity of interpolating functions is enforced in a similar manner by using quadratic Lagrange basis on tetrahedra with constraints at non-conforming junctions to match tri-linear hexahedra. The so-defined function spaces are validated numerically on simple Poisson and linear elasticity problems for which an analytical solution is known. We observe that using a hybrid mesh with the proposed function spaces results in an accuracy significantly better than when using linear tetrahedra and slightly worse than when solely using tri-linear hexahedra. As a consequence, the proposed function spaces may be a promising alternative for complex geometries that are out of reach of existing full hexahedral meshing methods.

Keywords: finite element method, hex-dominant mesh, hybrid mesh, continuous function space, hexahedral-tetrahedral mesh

1. Introduction and related work

In finite element methods, it is widely known that hexahedron finite elements achieve better execution-time than tetrahedra ones for reaching a given accuracy. Automatic tetrahedral meshing techniques are now mature and work well on any complex 3D model [1], [2]. On the contrary, hexahedral meshing is still an open and difficult problem for which there is still no satisfactory solution [3]. Difficulties in hexahedral meshing can be partially resolved by introducing other elements such as tetrahedra, pyramids and prisms, thus generating hybrid meshes. Recent progress in hexahedral-dominant meshing techniques such as [4], [5], [6] and [7] make it possible to automatically produce hybrid meshes with a large majority of hexahedra for arbitrary 3D models.

Recently in the context of discontinuous Galerkin methods, hybrid meshes have been successfully used on acoustic wave equation problems [8] or on Maxwell equations [9] with significant speedups over tetrahedral meshes. For standard Galerkin methods, continuous finite element spaces for hybrid meshes have been introduced, such as in [10]. A succinct survey exposing various approaches with emphasis on the pyramidal element is available in the introduction of [11]. All these propositions involve special functions, such as rationals, as it is not possible to build a polynomial function basis on the pyramid which is conforming with tetrahedra and hexahedra polynomial function basis, as noticed in [12].

In the present article, we adopt a different approach in which we consider hybrid meshes composed only of hexahedra and tetrahedra, for which finite element behavior is very well understood. A second interesting point of this approach is that enabling non-conforming hexahedra-tetrahedra junctions provides more flexibility to hex-dominant meshing techniques, resulting in a higher proportion of hexahedra, as it eliminates constraints associated with the generation of pyramids. However, without special care, non-conformities in the mesh result in a discontinuous geometry and a discontinuous function space.

The idea of using non-conforming hexahedral-tetrahedral meshes is not new and has been successfully developed in the context of the discontinuous Galerkin Method in electromagnetic in [13], [14] and [15]. For continuous Galerkin methods, constraints to ensure continuity of the divergence and of the rotational along non-conforming interfaces have been briefly proposed in [16]. In a engineering approach, hexahedra-tetrahedra non-conforming junction have been firstly discussed in [17] which proposes various multi-point constraints to ensure the function continuity or to minimize the error, depending of the finite element considered in their software. An

extention of this approach [18] discards non-conforming hexahedral-tetrahedral junctions in favor of pyramidal elements. Our contribution is to give a formal approach to this problem and to deal with the geometric discontinuity arising with non-planar hexahedra faces, which was not considered in previous work to our knowledge.

It should also be noted that previous works on finite element over hybrid meshes usually consider applications where hexahedral and tetrahedral elements lie in distinct regions. Transitional elements or non-conforming junctions arises then in localized layers or regions. This approach is especially efficient for problems such as acoustic where complex objects are meshed with tetrahedra and the propagation medium with hexahedra. Our approach is more oriented toward hex-dominant meshes where tetrahedra are located randomly in the mesh, resulting in a high number of non-conforming junctions scattered randomly in the domain.

In the present article, we introduce low-order continuous function spaces defined on hybrid non-conforming hexahedral-tetrahedral meshes. The geometric conformity is obtained by using quadratic mappings for tetrahedra to exactly fit the hexahedra non-planar faces. Likewise, quadratic Lagrange basis and constraints are used on tetrahedra to produce functions which are continuous (C^0) at interfaces with the tri-linear functions used in hexahedra.

2. Continuous function spaces on hybrid hexahedral-tetrahedral meshes

Our first goal is to deliver a *continuous* geometry for the mesh, in the sense explicited below. We will then explain how to define a *continuous* function space on this geometry.

Input. The input is a mesh composed of a set of vertices (geometric information) and a set of elements defined by their vertices and faces (combinatorial information). In the present article, we restrict ourselves to meshes that satisfy the following specification:

Definition 2.1. *Combinatorial hybrid hexahedral-tetrahedral mesh specification*
The input hybrid mesh $\mathcal{M}$ is composed of a set $\mathcal{P}$ of vertices, defined by their coordinates, a set of tetrahedra defined by their 4 vertices in $\mathcal{P}$, and a set of hexahedra defined by their 8 vertices in $\mathcal{P}$ and their 6 faces (defined by 4 vertices in $\mathcal{P}$). The connectivity is restricted to the following combinatorial cases:

- *Two tetrahedra share 0, 1, 2 or 3 vertices.*

- *Two hexahedra share 0, 1, 2 or 4 vertices. When they share 2 vertices, this is a common edge. When they share 4 vertices, this a common face.*
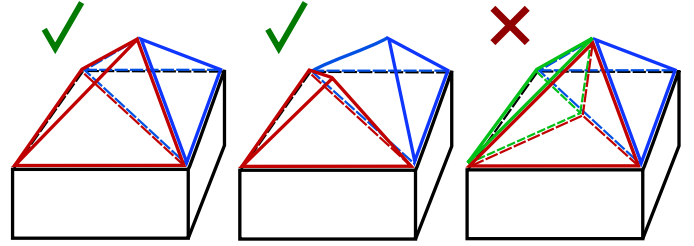

Figure 1: Supported and not supported non-conforming junctions between hexahedra and tetrahedra

- *One hexahedron and one tetrahedron share 0, 1, 2 or 3 vertices. When they share 3 vertices, there exists another tetrahedron which also shares 3 vertices with the hexahedron and two or three vertices with the tetrahedron. So in this setup, the hexahedron face is connected to 2 tetrahedra faces.* □

This specification permits non-conforming connections between a hexahedron and two tetrahedra, that we often refer as hybrid junction. But it excludes all other types of non-conforming connections. Examples of supported and not supported configurations are shown in figure 1.

2.1. Mesh geometry
The input mesh, defined by its combinatorial information, does not provide a geometry. A naive idea would be to use affine tetrahedra and tri-affine hexahedra but this solution leads to gaps or overlaps between hexahedra and tetrahedra at non-conforming junctions when hexahedron faces are not planar (see figure 2a.). The mesh geometry we are looking for should satisfy definition 2.2.

Definition 2.2. *Geometric hybrid hexahedral-tetrahedral mesh*
A hybrid hexahedral-tetrahedral mesh is the union of a set of (non-degenerate) hexahedra and of a set of (non-degenerate) tetrahedra. The cell geometries K_c of Ω_h satisfy:

- $\Omega_h = \bigcup_{i=c}^{N} K_c$

- *the intersection $K_i \cap K_j$ of two distinct tetrahedra is either empty, or reduced to a common vertex, or an entire common edge, or an entire common face (triangle)*

- *the intersection $K_i \cap K_j$ of two distinct hexahedra is either empty, or reduced to a common vertex, or an entire common edge, or an entire common face (quadrilateral)*

- *the intersection $K_i \cap K_j$ of an hexahedron and a tetrahedron is either empty, or a common vertex, or an entire common edge, or an entire quadrilateral diagonal, or a triangle such that there exists another tetrahedra K_l which intersection with K_i, $K_i \cap K_l$, is another tetrahedron face and $K_i \cap (K_j \cup K_l)$ is a quadrilateral face of K_i* □
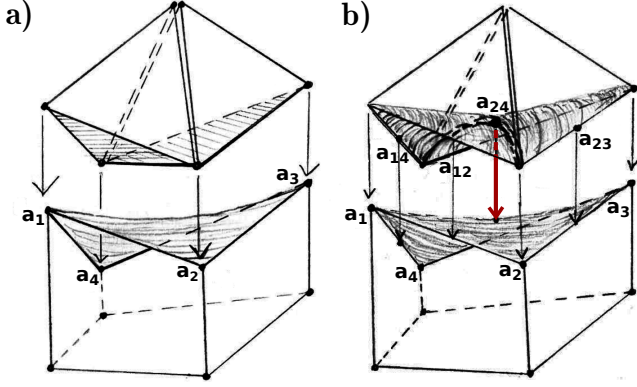
Figure 2: Non-conforming hexahedron-tetrahedra junction. a) Tetrahedra affine mappings, b) Tetrahedra quadratic mappings

Figure 3: Quadratic mapping of the reference tetrahedron

Following the standard finite element approach, we define cells as images of the reference tetrahedron $\hat{T}$ and of the reference hexahedron $\hat{Q}$ (detailed in appendices) by one-to-one mapping functions $\mathbf{F}_c$:

$$K_c = \mathbf{F}_c(\hat{T}) \text{ if the cell } c \text{ is a tetrahedron}$$

$$K_c = \mathbf{F}_c(\hat{Q}) \text{ if the cell } c \text{ is a hexahedron}$$

The edges and the faces in the definition 2.2 are images of edges and faces of the reference hexahedron or tetrahedron (so they can be curved).

The first question we consider is how to define the mappings $\mathbf{F}_c$, for both tetrahedra and hexahedra, in order to satisfy the general definition 2.2 (geometric continuity).

Hexahedron mappings. Let us start by considering the mapping $\mathbf{F}_Q$ of a hexahedron $K_q \in \Omega_h$. The standard mapping from the reference hexahedron $\hat{Q}$ (unit cube) is the so-called tri-affine mapping. It is based on the function space of polynomials of degree one in each variable $\mathbb{Q}_1$. Each component $F_{Q,j}$ is in $\mathbb{Q}_1$ so $\mathbf{F}_Q$ is in $(\mathbb{Q}_1)^3$. We have the decomposition:

$$\forall \hat{\mathbf{p}} \in \hat{Q}, \quad \mathbf{F}_Q(\hat{\mathbf{p}}) = \sum_{i=1}^{8} \mathbf{a}_i \ \hat{\psi}_i(\hat{\mathbf{p}})$$

where $(\hat{\psi}_i)_{i=1..8}$ is the basis of $\mathbb{Q}_1$ detailed in the appendix Appendix A.2 and $\mathbf{a}_i$ are the vertices of the hexahedron Q given in the input mesh.

It is important to notice that this tri-affine mapping has components which are polynomials of degree 3 (product of three degree one). If we consider the restriction to a face of $\hat{Q}$, then the restricted mapping is bi-affine, i.e. a bivariate polynomial of degree 2. It implies that the surface of the mapped face is a quadric, specifically a hyperbolic paraboloid. So for an arbitrary hexahedron, its faces are not planar in general.

This is not an issue for meshes composed only of hexahedra because they share common vertices at element junctions. But for hybrid hexahedral-tetrahedral mesh, it
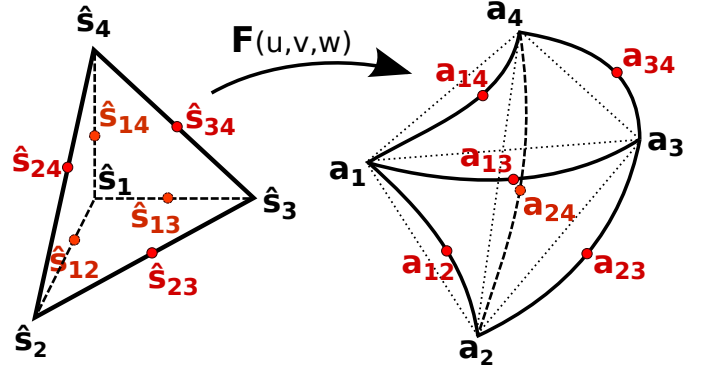
will not always be possible to glue two tetrahedra (planar faces) with a tri-affine hexahedron, which faces are quadric surfaces. This incompatibility is illustrated in the figure 2a. Unfortunately, automated hex-dominant mesh generation algorithms, such as [6], produce hexahedra with non-planar faces most of the time as they solely use combinatorial definitions. Therefore, we need to take these particularities into account in our finite element mappings.

Tetrahedron mappings. The simplest mapping $\mathbf{F}_T$ for an arbitrary tetrahedron is the affine one, where the three components lie in the space of polynomials of degree one $\mathbb{P}_1$. However this mapping generates faces which are planar, so it would not be possible in general to continuously connect a tetrahedron to an arbitrary hexahedron (which faces are quadric).

We propose to solve this issue by using quadratic mappings for tetrahedra (see figure 3). It allows us to deform tetrahedra geometry in order to fit exactly with the quadric hexahedron faces at hybrid interfaces.

Consider the mapping $\mathbf{F}_T$ which maps the reference tetrahedron $\hat{T}$ to the actual tetrahedron T. Instead of taking $\mathbf{F}_T$ in $(\mathbb{P}_1)^3$, we take $\mathbf{F}_T$ in $(\mathbb{P}_2)^3$, where $\mathbb{P}_2$ is the space of polynomials of degree 2, detailed in the appendix Appendix A.1. We have the decomposition:

$$\mathbf{F}_T = \sum_{i=1}^{4} \mathbf{a}_i \ \hat{\phi}_i + \sum_{1 \leq i < j \leq 4} \mathbf{a}_{ij} \ \hat{\phi}_{ij}$$

where the $\mathbf{a}_i$'s are the vertices of the tetrahedron T given in the input mesh, the $\mathbf{a}_{ij}$'s are the midpoints of edges $i-j$ and $(\hat{\phi}_i, \hat{\phi}_{ij})_{i,ij}$ is the basis of $\mathbb{P}_2$ detailed in the appendix Appendix A.1.

By moving the midpoints $\mathbf{a}_{ij}$, it is possible to control the deviation from the affine tetrahedron of the geometry, as shown in figure 3. Initially, the $\mathbf{a}_{ij}$ are set as $\mathbf{a}_{ij} = \frac{\mathbf{a}_i + \mathbf{a}_j}{2}$, this reproduces the affine mapping but we now have the freedom to change one of these coefficients to deform the geometry of tetrahedra.

We assume that the $\mathbf{a}_{ij}$ coefficients are chosen in such way that $\mathbf{F}_T$ remains a one-to-one mapping. This is the

3

case if the deviation from the actual edge midpoint is sufficiently small. For a more detailed discussion on the quadratic geometry validity, one can refer to [19]. This type of curved geometry, often referred to as isoparametric elements, is used in the finite element framework to produce meshes that better fit non-polygonal boundaries of 3D models.

At this point, the mesh geometry is defined by:

$$\Omega_h = \bigcup_c K_c \text{ with}$$

$$K_c = \mathbf{F}_c(\hat{T}), \ F_c \in (\mathbb{P}_2)^3 \text{ if } K_c \text{ is a tetrahedron}$$

$$K_c = \mathbf{F}_c(\hat{Q}), \ F_c \in (\mathbb{Q}_1)^3 \text{ if } K_c \text{ is a hexahedron}$$

To satisfy definition 2.2, we need to constrain the new degrees of freedom in tetrahedra (edge midpoints) at hybrid interfaces to ensure that the elements match exactly.

Continuity of the geometry at interfaces between elements.

1. For two connected hexahedra, both geometries match on the common face because both tri-affine mappings are fully determined by their values at reference vertices, and these values are nothing else than the hexahedron vertices of the combinatorial definition of the input mesh.

2. At the interface between two connected tetrahedra defined by quadratic mappings, the geometry continuity is achieved if both quadratic mappings share 6 coefficients, associated with values taken at vertices and edge midpoints of faces of the reference tetrahedron. Three of these equalities, at vertices, are guaranteed by the input mesh specification 2.1. The last three, at edge midpoints of reference faces, are added as constraints to our geometric mesh definition. This constraint is referred as ($\mathcal{C}$-T).

3. For hybrid hexahedron-tetrahedron interface, such as in figure 2, the key to achieve the continuity is to set the coefficient which corresponds to the hexahedron face diagonal to the point at the center of the face in both tetrahedra mappings. In figure 2b., $\mathbf{a}_{24}$ is set to $\frac{\mathbf{a}_1+\mathbf{a}_2+\mathbf{a}_3+\mathbf{a}_4}{4}$ instead of $\frac{\mathbf{a}_2+\mathbf{a}_4}{2}$. Other tetrahedra mapping coefficients associated with edge midpoints, such as a_{23}, are left at actual edge midpoints. The formalisation of this claim is given by the proposition 2.1.

Notations To lighten formulas, we adopt the following convention: the pre-images of vertices $\mathbf{a}_i$ of the mesh by element mappings $\mathbf{F}_e$ are denoted by $\hat{\mathbf{a}}_i = \mathbf{F}_e^{-1}(\mathbf{a}_i)$. These $\hat{\mathbf{a}}_i$ are vertices of the reference elements. When more than one mapping is involved in a formula, the right mapping can be deduced from the domain of the function which applies to $\hat{\mathbf{a}}_i$. One should be careful that it implies that in the same formula, two reference points denoted by $\hat{\mathbf{a}}_i$ can refer to two distinct points (but by renumbering of

nodes in the mappings, it is always possible to get to a configuration where both refer to the same point).

Proposition 2.1. *Non-conforming hexahedron-tetrahedra junction*
Let Q be a hexahedron defined by the tri-affine mapping $\mathbf{F}_Q$ of the reference hexahedron such that $\mathbf{a}_1, \mathbf{a}_2, \mathbf{a}_3, \mathbf{a}_4$ are the vertices of the face Σ_q of Q.
Let T be a tetrahedron defined by the quadratic mappings $\mathbf{F}_T$ of the reference tetrahedron such that $\mathbf{a}_1, \mathbf{a}_2, \mathbf{a}_3$ are the vertices of the face Σ_t of T.
Then $\Sigma_t \subset \Sigma_q$, i.e. the geometry of $Q \cup T$ is continuous, if

- *For common edges $[\mathbf{a}_i, \mathbf{a}_j]$, $(i,j) = (1,2), (1,4)$*

$$\mathbf{F}_T(\frac{\hat{\mathbf{a}}_i + \hat{\mathbf{a}}_j}{2}) = \frac{\mathbf{a}_i + \mathbf{a}_j}{2}$$

- *For the diagonal (a_2, a_4) of the face Σ_q, which is also a edge of Σ_t:*

$$\mathbf{F}_T(\frac{\hat{\mathbf{a}}_2 + \hat{\mathbf{a}}_4}{2}) = \frac{\mathbf{a}_1 + \mathbf{a}_2 + \mathbf{a}_2 + \mathbf{a}_4}{4}$$

Proof. See supplemental material. $\square$

The final mesh geometry with an explicit definition of the mappings is given by the following definition.

Definition 2.3. *Let $\mathcal{M}$ be the input combinatorial hybrid mesh which satisfies the specifications 2.1. For each element of $\mathcal{M}$, vertices are denoted by $\mathbf{a}_j$ where j is the local index. $\hat{\mathbf{a}}_j$ is the pre-image by the mapping $\mathbf{F}_i$ of the associated element.*
The space partition of Ω is the union $\Omega_h = \bigcup_{i=1}^{N} K_i$. The N element geometries are defined by the following mappings $(\mathbf{F}_i)_{i=1..N}$:

- *If the i-th element is a hexahedron, $K_i = \mathbf{F}_i(\hat{Q})$ with $\mathbf{F}_i \in (\mathbb{Q}_1)^3$ determined by $\mathbf{F}_i(\hat{\mathbf{a}}_j) = \mathbf{a}_j$, $1 \le j \le 8$*

- *If the i-th element is a tetrahedron, $K_i = \mathbf{F}_i(\hat{T})$ with $\mathbf{F}_i \in (\mathbb{P}_2)^3$ determined by $\mathbf{F}_i(\hat{\mathbf{a}}_j) = \mathbf{a}_j$, $1 \le j \le 4$ and for $1 \le j < k \le 4$:*

  - *$\mathbf{F}_i(\frac{\hat{\mathbf{a}}_j + \hat{\mathbf{a}}_k}{2}) = \frac{\mathbf{a}_j + \mathbf{a}_k + \mathbf{a}_l + \mathbf{a}_f}{4}$ if $(\mathbf{a}_j, \mathbf{a}_k)$ is a diagonal of a hexahedron face, whose vertices are $\mathbf{a}_j, \mathbf{a}_l, \mathbf{a}_k, \mathbf{a}_f$.*

  - *$\mathbf{F}_i(\frac{\hat{\mathbf{a}}_j + \hat{\mathbf{a}}_k}{2}) = \frac{\mathbf{a}_j + \mathbf{a}_k}{2}$ else*

This definition 2.3 satisfies both constraints ($\mathcal{C}$-T) at tetrahedra interfaces and the assumptions of the proposition 2.1 at hybrid interfaces. So a mesh geometry defined by 2.3 satisfies the definition 2.2 (continuity of the geometry).

2.2. Continuity of the function spaces

From now on, we assume that Ω_h is a partition of the domain Ω given by the definition 2.3. The objective is to use the hybrid mesh Ω_h to build a function space, in which functions are piecewise defined (element by element). Following the standard finite element approach of Ciarlet [20], we use two ingredients: function spaces described on reference elements and one-to-one element mappings. More specifically:

1. For our hybrid function space, we use the low-order polynomial spaces $\mathbb{Q}_1$ and $\mathbb{P}_2$ which have simple Lagrange-based basis $(\hat{\psi}_i)_{i=1..8}$, $(\hat{\phi}_i)_{i=1..10}$, defined respectively on the reference hexahedron $\hat{Q}$ and the reference tetrahedron $\hat{T}$ (see appendix).

2. The inverses of the element mappings defined in 2.3 are used to get to the reference elements from anywhere in the actual mesh Ω_h:

$$\forall \mathbf{p} \in \Omega_h, \qquad \exists \mathbf{F}_Q \in (\mathbb{Q}_1)^3 \text{ such that } \hat{\mathbf{p}} = \mathbf{F}_Q^{-1}(\mathbf{p}) \in \hat{Q}$$
$$\text{or} \quad \exists \mathbf{F}_T \in (\mathbb{P}_2)^3 \text{ such that } \hat{\mathbf{p}} = \mathbf{F}_T^{-1}(\mathbf{p}) \in \hat{T}$$

Note that in practice, the inverse mappings never need to be computed explicitly (see section 3.1).

Consider a hexahedron $K_q \in \Omega_h$ and a function $\hat{f} \in \mathbb{Q}_1$ defined by its values $(f_i)_{i=1..8}$ at the 8 vertices $\hat{q}_i$ of $\hat{Q}$. Then by composition, we form the function $f_{|K_q}$ defined by:

$$\forall \mathbf{p} \in K_q, \ f_{|K_q}(\mathbf{p}) = \hat{f} \circ F_Q^{-1}(\mathbf{p}) = \hat{f}(\hat{\mathbf{p}})$$

The same construction can be done for a tetrahedron $K_t \in \Omega_h$ by taking $\hat{f} \in \mathbb{P}_2$. So our space is composed of functions, whose restrictions on each elements are defined by the composition of a polynomial (in $\mathbb{Q}_1$ or in $\mathbb{P}_2$) and the inverse mapping of the element. We name it $\mathrm{D}\mathcal{H}yb_{12}$, for discontinuous hybrid space:

$$\mathrm{D}\mathcal{H}yb_{12} = \{f \in L^2(\Omega_h) \text{ such that } f_{|K_c} = \hat{f} \circ F_{K_c}^{-1},$$
$$\hat{f} \in \mathbb{Q}_1 \text{ if } K_c \in \Omega_h \text{ is a hexahedron}$$
$$\hat{f} \in \mathbb{P}_2 \text{ if } K_c \in \Omega_h \text{ is a tetrahedron}\}$$

On each element, the functions of this space are continuous (composition of a polynomial and a continuous mapping). The continuity at element interfaces needs to be enforced (see below).

Remark 2.1. *It is important to notice that the space $\mathrm{D}\mathcal{H}yb_{12}$ is not composed of polynomials, because if mapping components are polynomials (of degree 2), inverse mappings are not.*

As stated in the section introduction, our goal is to build a *continuous* function space $\mathcal{H}yb \subset \mathcal{C}^0(\Omega)$ which is suitable for classic finite element methods. We achieve this by adding constraints at interfaces between elements in $\mathrm{D}\mathcal{H}yb_{12}$. We propose two continuous function spaces: $\mathcal{H}yb_{12}$ and $\mathcal{H}yb_1$. $\mathcal{H}yb_{12}$ is the space with the minimum

of constraints applied to $\mathrm{D}\mathcal{H}yb_{12}$ to ensure continuity and $\mathcal{H}yb_1$ is a space with more constraints but easier to manipulate, more in the spirit of our initial objectives.

Let us look at interfaces between elements to determine explicitly the constraints. We only consider surface interfaces because continuity at edges is guaranteed by continuity at surface interfaces.

Continuity conditions at element surface interfaces.

1. *Between two hexahedra.* A function $f \in \mathrm{D}\mathcal{H}yb_{12}$ is continuous at a hexahedra interface if its restrictions to both elements are equal at the common face vertices. Below is a more detailed explanation:

Let consider two connected hexahedra Q_1, Q_2 which share the face Σ_q, with vertices $\mathbf{a}_1, \mathbf{a}_2, \mathbf{a}_3, \mathbf{a}_4$. The tri-affine mappings are respectively $\mathbf{F}_1$ and $\mathbf{F}_2$. The pre-images of the face by the mappings are denoted by $\hat{\Sigma}_1 = \mathbf{F}_1^{-1}(\Sigma_q)$, $\hat{\Sigma}_2 = \mathbf{F}_2^{-1}(\Sigma_q)$.

The restrictions to the common face $f_{|Q_1 \cap \Sigma_q}, f_{|Q_2 \cap \Sigma_q}$ can be decomposed as: $f_{|Q_1 \cap \Sigma_q} = \hat{f}_{1|\hat{\Sigma}_1} \circ \mathbf{F}_{1|\Sigma_q}^{-1}$ and $f_{|Q_2 \cap \Sigma_q} = \hat{f}_{2|\hat{\Sigma}_2} \circ \mathbf{F}_{1|\Sigma_q}^{-1}$. Both $\hat{f}_{1|\Sigma_1}, \hat{f}_{2|\Sigma_2}$ are determined by their values at vertices of $\hat{\Sigma}_1, \hat{\Sigma}_2$ (see appendix). So both restrictions are equal if

$$\forall i \in [1,4], \qquad \hat{f}_{1|\hat{\Sigma}_1}(\mathbf{F}_1^{-1}(\mathbf{a}_i)) = \hat{f}_{2|\hat{\Sigma}_2}(\mathbf{F}_2^{-1}(\mathbf{a}_i))$$
$$\Leftrightarrow \quad f_{|Q_1}(\mathbf{a}_i) = f_{|Q_2}(\mathbf{a}_i)$$

We denote $(\mathcal{C}\text{-I})$ this continuity condition at hexahedra interfaces Using the notation convention introduced for proposition 2.1, this can be re-written as:

$$\forall i \in [1,4], \quad \hat{f}_{1|\hat{\Sigma}_1}(\hat{\mathbf{a}}_i) = \hat{f}_{2|\hat{\Sigma}_2}(\hat{\mathbf{a}}_i)$$

2. *Between two tetrahedra.* A function $f \in \mathrm{D}\mathcal{H}yb_{12}$ is continuous at a tetrahedra interface if its values are equal at the three vertices and at the three edge midpoints of the common face. More specifically:

Let consider two connected tetrahedra T_1, T_2 which share the face Σ_q, with vertices $\mathbf{a}_1, \mathbf{a}_2, \mathbf{a}_3$. The quadratic mappings are respectively $\mathbf{F}_1$ and $\mathbf{F}_2$. The restrictions $f_{|T_1 \cap \Sigma_q}, f_{|T_2 \cap \Sigma_q}$ are determined by their values at the three vertices and at the three edge midpoints of the pre-images of Σ_q by the mappings (see appendix), denoted by $\hat{\Sigma}_1 = \mathbf{F}_1^{-1}(\Sigma_q)$, $\hat{\Sigma}_2 = \mathbf{F}_2^{-1}(\Sigma_q)$. Both restrictions are equal if:

- For common vertices $a_i, \ i \in 1, 2, 3$:

$$\hat{f}_{1|\hat{\Sigma}_1}(\hat{\mathbf{a}}_i) = \hat{f}_{2|\hat{\Sigma}_2}(\hat{\mathbf{a}}_i)$$

- For common edges $[a_i, a_j], \ (i,j) = (1,2), (1,3), (2,3)$:

$$\hat{f}_{1|\hat{\Sigma}_1}\left(\frac{\hat{\mathbf{a}}_i + \hat{\mathbf{a}}_j}{2}\right) = \hat{f}_{2|\hat{\Sigma}_2}\left(\frac{\hat{\mathbf{a}}_i + \hat{\mathbf{a}}_j}{2}\right)$$

5

We denote ($\mathcal{C}$-II) this continuity condition at tetrahedra interfaces.

3. *Between one hexahedron and one tetrahedron.* A function $f \in \mathrm{D}\mathcal{H}yb_{12}$ is continuous at a non-conforming hexahedron-tetrahedron interface if its values are equal at the three common vertices, at the two common edge midpoints and at the quadrilateral center, which is a edge midpoint of the triangle. We formalize this last continuity condition ($\mathcal{C}$-III) with proposition 2.2:

Proposition 2.2. *Continuity of the function spaces at hybrid junctions*
Let Q be a hexahedron and T be a tetrahedron which share the triangular face Σ_t (vertices $\mathbf{a}_1, \mathbf{a}_2, \mathbf{a}_4$) of T. The associated quadrilateral face of Q is denoted by Σ_q (vertices $\mathbf{a}_1, \mathbf{a}_2, \mathbf{a}_3, \mathbf{a}_4$). This configuration is shown in figure 2b.. The element mappings $\mathbf{F}_Q, \mathbf{F}_T$ satisfy the mesh definition 2.3.
Let $f_h \in \mathrm{D}\mathcal{H}yb_{12}$. Its restrictions $f_{|Q}, f_{|T}$ are defined by the compositions $f_{|Q} = \hat{f}_Q \circ \mathbf{F}_Q^{-1}$ and $f_{|T} = \hat{f}_T \circ \mathbf{F}_T^{-1}$.
f_h is continuous at the hybrid interface Σ_t, i.e. $f_{|T \cap \Sigma_t} = f_{|Q \cap \Sigma_q}$ on Σ_t, if:

1. *At common vertices $\mathbf{a}_i$, $i \in 1, 2, 4$:*

$$\hat{f}_T(\hat{\mathbf{a}}_i) = \hat{f}_Q(\hat{\mathbf{a}}_i)$$

(these points are degree of freedom for both functions $\hat{f}_Q \in \mathbb{Q}_1, \hat{f}_T \in \mathbb{P}_2$)

2. *At common edges $(\mathbf{a}_i, \mathbf{a}_j)$, $(i,j) = (1,2), (1,4)$:*

$$\hat{f}_T(\frac{\hat{\mathbf{a}}_i + \hat{\mathbf{a}}_j}{2}) = \hat{f}_Q(\frac{\hat{\mathbf{a}}_i + \hat{\mathbf{a}}_j}{2})$$

(these points are degree of freedom only for $\hat{f}_T \in \mathbb{P}_2$)

3. *At the diagonal $(\mathbf{a}_2, \mathbf{a}_4)$ of Σ_q:*

$$\hat{f}_T(\frac{\hat{\mathbf{a}}_2 + \hat{\mathbf{a}}_4}{2}) = \hat{f}_Q(\frac{\hat{\mathbf{a}}_1 + \hat{\mathbf{a}}_2 + \hat{\mathbf{a}}_3 + \hat{\mathbf{a}}_4}{4})$$

(this point is a degree of freedom only for $\hat{f}_T \in \mathbb{P}_2$)

Proof. See supplemental material. $\square$

By solely considering functions $f \in \mathrm{D}\mathcal{H}yb_{12}$ which satisfy conditions ($\mathcal{C}$-I), ($\mathcal{C}$-II), ($\mathcal{C}$-III), we form the function space $\mathcal{H}yb_{12}$ defined as follow:

Definition 2.4. *Continuous hybrid hexahedral-tetrahedral function space*
Let Ω_h a partition of Ω which satisfies definition 2.3.

$$\mathcal{H}yb_{12} = \{v \in \mathcal{C}^0(\Omega_h) \text{ such that } v_{|K_i} = \hat{v} \circ F_{K_i}^{-1}$$
$$\hat{v} \in \mathbb{P}_2 \text{ if } K_i \text{ is a tetrahedron}$$
$$\hat{v} \in \mathbb{Q}_1 \text{ if } K_i \text{ is a hexahedron}\}$$

It should be stressed that the space $\mathcal{H}yb_{12}$ is composed of functions formed from $\mathbb{Q}_1$ and $\mathbb{P}_2$. But as in practice the proportion of tetrahedra is low, most tetrahedra are connected to hexahedra and their degree of freedom on edge midpoints are constrained and do not contribute to the solution approximation. Considering this remark, it can be interesting to also remove the remaining edge midpoint degrees of freedom at tetrahedra interfaces. This produces a smaller continuous function space that we call $\mathcal{H}yb_1$. In practice it is achieved by changing the continuity condition ($\mathcal{C}$-II) to a more constraining one, denoted by ($\mathcal{C}$-II-b), which forces function values at tetrahedra edge midpoints to be the average of function values at edge vertices (when these edges are not hexahedron face diagonal). The second point of ($\mathcal{C}$-II) becomes:

- At common edges $[a_i, a_j]$ of tetrahedra interfaces which are not hexahedron face diagonal:

$$\hat{f}_{1|\hat{\Sigma}_1}(\frac{\hat{\mathbf{a}}_i + \hat{\mathbf{a}}_j}{2}) = \hat{f}_{2|\hat{\Sigma}_2}(\frac{\hat{\mathbf{a}}_i + \hat{\mathbf{a}}_j}{2})$$
$$= \frac{\hat{f}_{1|\hat{\Sigma}_1}(\hat{\mathbf{a}}_i) + \hat{f}_{1|\hat{\Sigma}_1}(\hat{\mathbf{a}}_j)}{2} = \frac{\hat{f}_{2|\hat{\Sigma}_2}(\hat{\mathbf{a}}_i) + \hat{f}_{2|\hat{\Sigma}_2}(\hat{\mathbf{a}}_j)}{2}$$

With this condition ($\mathcal{C}$-II-b), the resulting function space $\mathcal{H}yb_1$ is still continuous but function restrictions to tetrahedra which are not connected to hexahedra are formed from $\mathbb{P}_1$ (polynomials of degree 1). More importantly, functions in $\mathcal{H}yb_1$ are entirely defined by their values at mesh vertices, resulting in functions easier to manipulate and a smaller linear system in the finite element method.

Definition 2.5. *Minimal continuous hybrid hexahedral-tetrahedral function space*
Let Ω_h a partition of Ω which satisfies definition 2.3.

$$\mathcal{H}yb_1 = \{v \in \mathcal{H}yb_{12} \text{ that satisfy } (\mathcal{C}\text{-II-}b)\}$$

The introduced function spaces satisfy the following inclusions:
$$\mathcal{H}yb_1 \subset \mathcal{H}yb_{12} \subset \mathrm{D}\mathcal{H}yb_{12}$$
$$\mathcal{H}yb_1 \subset \mathcal{H}yb_{12} \subset \mathcal{C}^0$$

2.3. Function space basis

This section details explicitly the function basis of the space $\mathcal{H}yb_1$ and $\mathcal{H}yb_{12}$. One difficulty is these spaces have been built by using constraints that depend of the mesh local combinatorial configuration (element type, hybrid interface or not) and that cannot be applied blindly in a generic way. So it is not straightforward to expose the basis of $\mathcal{H}yb_1, \mathcal{H}yb_{12}$.

Consider the hybrid mesh $\mathcal{M}$ composed of n_v vertices $\mathbf{a}_i$ and n_{te} tetrahedra edges, which midpoints nodes are denoted by $\mathbf{a}_{ij}$ for edge $\mathbf{a}_i - \mathbf{a}_j$ (these midpoints satisfy the geometric continuity of the definition 2.3). We introduce two convenient notations:

– Sup($\mathbf{a}_i$) is the set of *cells* adjacent to $\mathbf{a}_i$.

– TSup($\mathbf{a}_{ij}$) denotes the set of *tetrahedra* which contains the edge $\mathbf{a}_i - \mathbf{a}_j$.

We use an intermediary function basis $((\psi_i)_i, (\psi_{ij})_{ij})$ made of a mix of $\mathbb{Q}_1, \mathbb{P}_2$ finite element basis. It is defined on each elements by:

- if $K \notin \mathrm{Sup}(\mathbf{a}_i)$: $\psi_{i|K} = 0$

- if $K \in \mathrm{Sup}(\mathbf{a}_i)$ and K is a hexahedron:
  $\psi_{i|K} = \hat{\psi}_i \circ \mathbf{F}_K^{-1}$, $\hat{\psi}_i \in \mathbb{Q}_1$ with $\hat{\psi}_i(\hat{\mathbf{a}}_j) = \delta_{ij}$
  (the $\hat{\mathbf{a}}_j$'s are the pre-images of K vertices by $\mathbf{F}_K$)

- if $K \in \mathrm{Sup}(\mathbf{a}_i)$ and K is a tetrahedron:
  $\psi_{i|K} = \hat{\psi}_i \circ \mathbf{F}_K^{-1}$, $\hat{\psi}_i \in \mathbb{P}_2$
  $\qquad\qquad$ with $\hat{\psi}_i(\hat{\mathbf{a}}_j) = \delta_{ij}$, $\hat{\psi}_i(\hat{\mathbf{a}}_{jk}) = 0$
  (the $\hat{\mathbf{a}}_j$'s are the pre-images of K vertices by $\mathbf{F}_K$ and the $\hat{\mathbf{a}}_{jk}$'s are the pre-images of the edge midpoints)

And

- if $K \notin \mathrm{TSup}(\mathbf{a}_{ij})$: $\psi_{ij|K} = 0$

- if $K \in \mathrm{TSup}(\mathbf{a}_{ij})$:
  $\psi_{ij|K} = \hat{\psi}_{ij} \circ \mathbf{F}_K^{-1}$, $\hat{\psi}_{ij} \in \mathbb{P}_2$
  $\qquad\qquad$ with $\hat{\psi}_{ij}(\hat{\mathbf{a}}_k) = 0$, $\hat{\psi}_{ij}(\hat{\mathbf{a}}_{kl}) = \delta_{ik}\delta_{jl}$
  (the $\hat{\mathbf{a}}_k$'s are the pre-images of K vertices by $\mathbf{F}_K$ and the $\hat{\mathbf{a}}_{kl}$'s are the pre-images of the edge midpoint nodes)

It should be noticed that ψ_i is discontinuous if $\mathbf{a}_i$ is the vertex of both a tetrahedron and of a hexahedron. ψ_{ij} is discontinuous if $\mathbf{a}_i$ and $\mathbf{a}_j$ are hexahedron vertices. One should also notice that the ψ_{ij} functions are always zeros on hexahedra. Think of them as correcting functions to recover continuity, only defined on tetrahedra.

To refer to previous sections, the space generated by this basis corresponds to $\mathrm{D}\mathcal{H}yb_{12}$ with constraints $(\mathcal{C}\text{-I}), (\mathcal{C}\text{-II})$ enforced. By the adding constraint $(\mathcal{C}\text{-III})$ at hybrid interfaces we ensure continuity and form $\mathcal{H}yb_{12}$. By adding $(\mathcal{C}\text{-II-b})$ at tetrahedra interfaces, we reduce the generated space to $\mathcal{H}yb_1$.

Consider the basis $(\phi_i)_{i=1..n_v}$ of $\mathcal{H}yb_1$ that has degrees of freedom only on mesh vertices. We explicit its functions using linear combination of ψ_i, ψ_{ij} that depend of the local combinatorial configuration in the hybrid mesh. We first need to introduce two more notations for edges:

– $\mathrm{ET}(\mathbf{a}_i)$ is the set of tetrahedron *edges* which contain $\mathbf{a}_i$ and which are not hexahedron face diagonal (this set can be empty).

– $\mathrm{ETD}(\mathbf{a}_i)$ is the set of tetrahedron *edges* such that the *tetrahedron* contains $\mathbf{a}_i$ and the edges are hexahedron face diagonal. This includes edges that do not contain $\mathbf{a}_i$.

We define ϕ_i on each element K by:

- if K is a hexahedron: $\phi_{i|K} = \psi_{i|K}$.

- if K is a tetrahedron:

$$\phi_{i|K} = \psi_{i|K}$$
$$+ \frac{1}{2} \sum_{\text{edge } ij \in \mathrm{ET}(\mathbf{a}_i)} \psi_{ij|K} + \frac{1}{4} \sum_{\text{edge } jk \in \mathrm{ETD}(\mathbf{a}_i)} \psi_{jk|K}$$

The last combination can be derived by continuity arguments: if $\mathbf{a}_i$ is the vertex of a hexahedron face, ϕ_i is equal to $1/2$ at edge $i - j$ midpoints of the face and is equal to $1/4$ at the face center. Now consider a tetrahedron which is connected to this face (by a triangular face containing $\mathbf{a}_i$ or by an edge containing $\mathbf{a}_i$ or by a quad diagonal containing $\mathbf{a}_i$ or not). At a connecting edge $j - k$, the only function of (ψ_i, ψ_{ij}) in the tetrahedron which is non-zero at $\mathbf{a}_{jk}$ is ψ_{jk} (which is equal to 1 at $\mathbf{a}_{jk}$). Applying this argument at all connecting edges of the tetrahedron set the coefficients of the linear combination as above.

Important remark The definition of the basis $(\phi_i)_{i=1..n_v}$ is tricky because when $\mathbf{a}_i$ is the vertex of a hybrid interface, and not on the diagonal, the function $\phi_{i|K}$ can be non-zero on a tetrahedron K which does not lie in $\mathrm{Sup}(\mathbf{a}_i)$. This is a consequence of the insertion of correcting functions at interface diagonals (via $\mathrm{ETD}(\mathbf{a}_i)$ in the definition) even when $\mathbf{a}_i$ does not lie on the diagonal. For instance, consider the figure 2b.), and let L be the top-left tetrahedron, R be the top-right tetrahedron and $\mathbf{a}_5$ be the top vertex, then:

$$\phi_{1|L} = \psi_{1|L} + \frac{1}{2}(\psi_{12|L} + \psi_{14|L} + \psi_{15|L}) + \frac{1}{4}\psi_{24|L}$$
$$\phi_{1|R} = \frac{1}{4}\psi_{24|R}$$

One should notice that $\phi_{1|R}$ is non-zero, so it has to be considered when computing the integrals in a finite element code. This makes the assembly of the matrices more complicated but this is required to recover the function continuity on a non-conforming mesh. $\qquad\square$

To form a basis of $\mathcal{H}yb_{12}$, one need to proceed with the same construction except for two changes:

– add functions ϕ_{ij} defined by $\phi_{ij|K} = \psi_{ij|K}$ at tetrahedra edges $j - k$ which are not hexahedron edges nor hexahedron face diagonal.

– relax the constraints: replace $\mathrm{ET}(\mathbf{a}_i)$ by $\mathrm{ETH}(\mathbf{a}_i)$, the set of tetrahedron *edges* which contain $\mathbf{a}_i$ *and which are hexahedron edges*, in the last point of the basis definition.

These explicit basis descriptions are useful when implementing the spaces $\mathcal{H}yb_1, \mathcal{H}yb_{12}$ in a finite element library: one can compute the local element contributions by combination of the standard $\mathbb{Q}_1, \mathbb{P}_2$ function space contributions.

2.4. Properties of the continuous function spaces

The most important property of $\mathcal{H}yb_{12}, \mathcal{H}yb_1$ is that they are subspaces of the Sobolev space H^1, because H^1 plays a fundamental role in the theory of partial differential equations, especially for the finite element method. Notably, it allows to apply the Lax-Milgram theorem (see [20]) that guarantees existence and uniqueness of the solutions of the weak formulations used in the application section.

Proposition 2.3. *Subspaces of Sobolev space*
Let Ω_h a hybrid mesh which satisfies the definition 2.3. Function spaces $\mathcal{H}yb_{12}, \mathcal{H}yb_1$, respectively defined by 2.4, 2.5, are subspaces of $H_1(\Omega_h)$.

Consequently, $\mathcal{H}yb_{12}, \mathcal{H}yb_1$ are Hilbert spaces.

Proof. The proof can be adapted from [21, p. 47]: the assumptions on the mesh change slightly but it does not affect the rest of the proof which relies on the continuity of the function space. $\square$

3. Examples of applications to partial derivate equations

In this section, we solve Poisson and the linear elasticity problems with the continuous function spaces $\mathcal{H}yb_{12}, \mathcal{H}yb_1$. For simple problems where the analytical solution is known, we compute errors in L^2-norm and compare to standard finite elements (tri-linear hexahedra $\mathbb{Q}_1$ and linear tetrahedra $\mathbb{P}_1$).

3.1. Poisson problem

Consider the following boundary value problem composed of the *Poisson equation* (1) subject to homogeneous Dirichlet boundary conditions (2).

$$-\Delta u = f \quad \text{in} \quad \Omega \tag{1}$$
$$u = 0 \quad \text{on} \quad \partial\Omega \tag{2}$$

where u is the unknown (temperature in heat equation for instance), f a source term and $\partial\Omega$ the domain boundary.

Weak formulation. Following the standard Galerkin approach, we project (1) onto a approximation space V to obtain the weak formulation (3).

$$\forall v \in V, \int_\Omega -\Delta u \; v \; \mathrm{d}x = \int_\Omega f \; v \; \mathrm{d}x \tag{3}$$

Since V is sufficiently regular, namely $V \subset C^0(\Omega) \cap H^1(\Omega)$ (this is the case for $\mathcal{H}yb_1, \mathcal{H}yb_{12}$), we can use integration by parts formula. The Dirichlet boundary condition is taken into account by restricting ourselves to $V_0 = \{v \in V \text{ such that } v = 0 \text{ on } \partial\Omega\}$. Thus the weak formulation becomes:

$$\forall v \in V_0, \int_\Omega \nabla u \; \nabla v \; \mathrm{d}x = \int_\Omega f \; v \; \mathrm{d}x \tag{4}$$

(see finite element textbooks such as [20], [22], [21] for detailed derivations and proofs)

Finite element discretization. We now consider the finite dimension subspace $V_h \subset V$, $V_h = \mathcal{H}yb_1$ or $V_h = \mathcal{H}yb_{12}$. Functions u and v can be both decomposed onto the $(\phi_i)_{i=1..n}$ function basis of V_h. Then (4) becomes a linear system of equations $Ax = B$ with:

$$A_{ij} = \int_\Omega \nabla\phi_i \nabla\phi_j \mathrm{d}x \quad \text{and} \quad B_i = \int_\Omega f\phi_i \mathrm{d}x$$

These integrals are decomposed over elements. For each element, a change of variable is used to get back to the reference element (and the chain rule if derivatives are involved). For instance, the contribution of element K_c to the coefficient B_i is:

$$B_{i|K_c} = \int_{\hat{K}_c} f(\mathbf{F}_{K_c}(\hat{\mathbf{x}})) \; \hat{\phi}_i(\hat{\mathbf{x}}) \; |\det(J_{\mathbf{F}_{K_c}}(\hat{\mathbf{x}}))| \mathrm{d}\hat{\mathbf{x}}$$

The integrals are computed using numerical quadrature, i.e. evaluating operand at well-chosen locations, so values taken by $\hat{\phi}_i, \nabla\hat{\phi}_i$ can be pre-computed on reference elements and used for computations on actual elements. For each element, one also needs to compute the Jacobian of the mappings at quadrature points (which is not constant for tri-affine and quadratic mappings).

Numerical validation on analytical Poisson problem. Consider the simple following Poisson problem on the unit cube $\Omega = [0, 1]^3$:

$$-\Delta u = 3\pi^2 sin(\pi x) * sin(\pi y) * sin(\pi z) \quad \text{in} \quad \Omega \tag{5}$$
$$u = 0 \quad \text{on} \quad \partial\Omega_D$$

Its analytical solution is $u = \sin(\pi x) * \sin(\pi y) * \sin(\pi z)$.

Numerical experiment setup. The meshes that we use are built using the following procedure: (a) the unit cube is regularly divided in smaller cubes, (b) vertices inside the cube are randomly displaced within a range up to d% of mean edge length, (c) some cubes are transformed into 6 tetrahedra. Distortion of the mesh (also used in [11]) applied in step (b) ensures elements are not parallel to borders and that hexahedra faces are not planar. This is an attempt to eliminate specific artefacts associated with unrealistic regularity of the mesh. Transformation of hexahedra into tetrahedra (step (c)) is used to generate hexahedral-tetrahedral meshes or fully tetrahedral meshes.

For numerical experiments, 20% of hexahedra are transformed in tetrahedra, resulting in a hybrid mesh where tetrahedra are 60% of overall elements. This proportion is largely superior to typical outputs of hex-dominant meshing algorithms. The distortion of interior vertices is set to $d = 10\%$, this produces dihedral angles with an average of 9 degrees and a maximum at 42 degrees for quadrilateral faces if we consider them as two triangles (see figure 2a.). From our experience with hex-dominant meshes [6], they are typical non-planarity angles. An example of hybrid mesh built with this procedure is shown in figure 4.
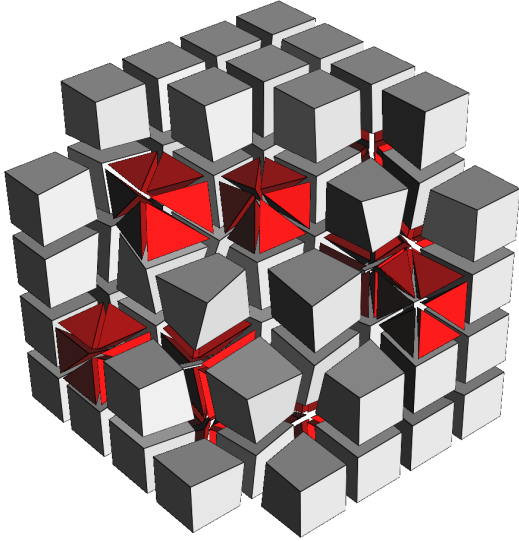
Figure 4: Example of hybrid hexahedral-tetrahedral mesh of the unit cube with distortion $d = 10\%$. The tetrahedra are colored in red and the hexahedra in grey.

Figure 5: Finite element simulation errors on Poisson analytical problem for different finite element spaces. $\mathcal{H}yb_1$ and $\mathcal{H}yb_{12}$ solutions are close to $\mathbb{Q}_1$ solutions and are significantly better than $\mathbb{P}_1$ solutions. Both axis use logarithmic scale.

Results. The function spaces $\mathcal{H}yb_1, \mathcal{H}yb_{12}$ have been implemented in a modified version of the open source library MFEM [23]. We solve the analytical problem (5) with finite element basis $\mathcal{H}yb_1, \mathcal{H}yb_{12}, \mathbb{P}_1, \mathbb{Q}_1$ on meshes successively refined. Relative errors in L^2-norm are reported in figure 5. In x-axis, we use (#degree of freedom)$^{\frac{1}{3}}$ which is proportional to inverse of the cell sizes in our cubic configuration.

We observe that error convergence rates are quadratic in L^2-norm with mesh refinement. For $\mathbb{P}_1, \mathbb{Q}_1$, this is the optimal convergence rate, see [20]. For $\mathcal{H}yb_1, \mathcal{H}yb_{12}$, this could be expected as they are made of $\mathbb{Q}_1$ and $\mathbb{P}_2$ with added linear constraints. The interesting part is hybrid function spaces are much more closer to $\mathbb{Q}_1$ than to $\mathbb{P}_1$. Measured accuracy with $\mathcal{H}yb_1$ is three times better than with $\mathbb{P}_1$. Thus solutions computed with the introduced spaces achieve good accuracy, 1% for instance, with much less refined meshes, and consequently smaller linear systems. Figure 6 shows the same computations with the elapsed times in x-axis. These timings include the assembly of the linear system and the solve time of the iterative conjugate gradient solver (reduction of the residual by a factor 10^{10}). These results still indicate a gain of $\mathcal{H}yb_1, \mathcal{H}yb_{12}$ spaces over $\mathbb{P}_1$. The timings obtained for small meshes (time < 0.5 seconds) do not carry useful information as they are too much influenced by external parameters such as processor cache, other jobs running, etc. It should also be reported that our implementation can be significantly improved as it currently uses a large linear system (corresponding to the non-constrained space) which is then reduced by applying constraints as matrix-matrix multiplications. This can be avoided by computing directly the right linear system to reduce execution-times, as suggested in section 2.3.
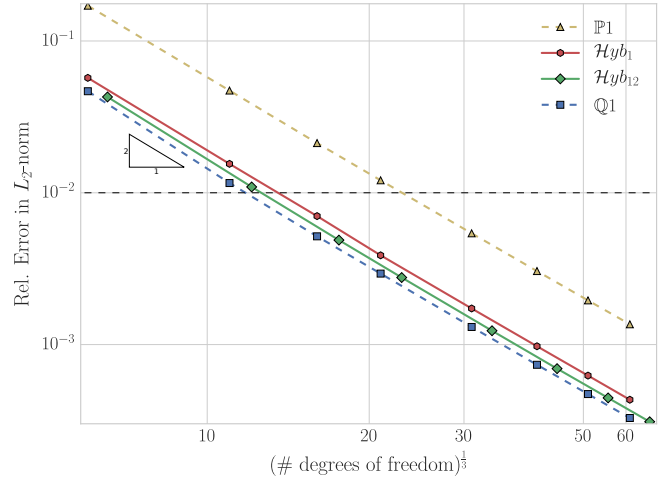
Importance of tetrahedra quadratic mappings. Quadratic mappings for tetrahedra at non-conforming interfaces (introduced in proposition 2.1 to recover the continuity of the geometry) can be seen as superfluous in the context of finite element simulations as there are other sources of numerical errors. To highlight their impact, we solve the same analytical problem with $\mathcal{H}yb_1$ using affine and quadratic mappings for distortion values $d = 10\%$ and $d = 20\%$. The results are reported in figure 7.

This experiment shows that for high accuracy (error $< 3\%$), the use of affine mappings instead of quadratic ones for tetrahedra of hybrid junctions can induce significant errors. As one can expect, this error is tightly linked to the degree of non-planarity of hexahedron faces. So our advice is to check the quality of hexahedron faces in a pre-processing phase, and if the quality is high (typically dihedral angle of quadrilateral faces < 5 degrees), the usage of affine mapping approximation is reasonable unless high accuracy is desired. An experiment with $\mathcal{H}yb_{12}$ exhibits exactly the same behavior (loss of convergence when using affine mappings).

3.2. Linear elasticity

The system of equations of linear elasticity is the usual description for continuum mechanics with small deformations. Consider a deformable medium Ω at equilibrium, fixed on $\partial\Omega_D$, subject to a volumetric load $\mathbf{f}$ inside Ω and to a surface force $\mathbf{g}$ on the boundary $\partial\Omega_N$. The material behavior is given by the Hooke's law (Lamé parameters λ, μ). The resulting displacement field $\mathbf{u} \in \mathbb{R}^3$ is governed
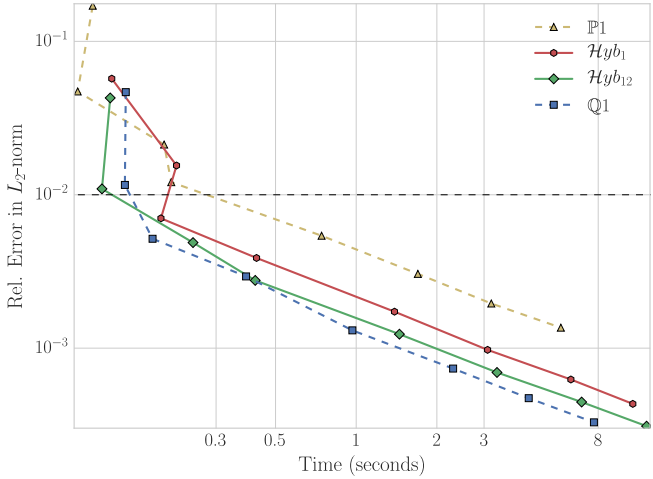
Figure 6: Relative errors in L^2-norm for various finite element spaces as functions of computing time (assembly + solver). Both axis use logarithmic scale.
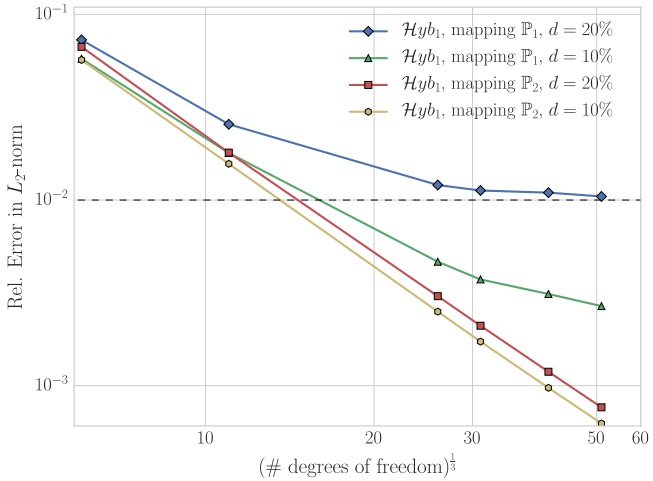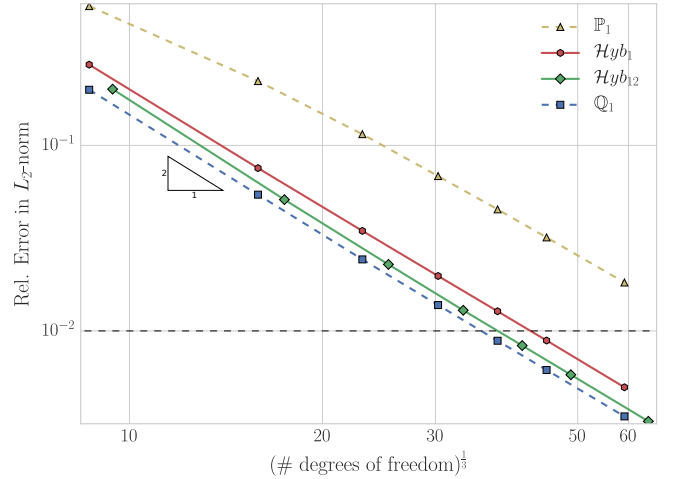

Figure 8: Finite element simulation error on linear elasticity analytical problem for different finite element spaces. $\mathcal{H}yb_1$ and $\mathcal{H}yb_{12}$ solutions are close to $\mathbb{Q}_1$ solutions and are significantly better than $\mathbb{P}_1$ solutions.

Figure 7: Influence of tetrahedra mappings at non-conforming interfaces on the analytical Poisson problem, for 10% and 20% edge length displacement of vertices in the cube. Affine mappings $\mathbb{P}_1$ and quadratic mappings $\mathbb{P}_2$.

other textbooks for the details.

$$\forall \mathbf{v} \in (V_0)^3, \int_\Omega \nabla \cdot \mathbf{u} \, \nabla \cdot \mathbf{v} + 2 \, \mu \, \epsilon(\mathbf{u}) : \epsilon(\mathbf{v}) \, \mathrm{d}x \qquad (10)$$
$$= \int_\Omega \mathbf{f} \cdot \mathbf{v} \, \mathrm{d}x + \int_{\partial\Omega_N} \mathbf{g} \cdot \mathbf{v} \, \mathrm{d}s$$

where $\epsilon(\mathbf{u}) = \frac{1}{2}(\nabla \cdot \mathbf{u} + \nabla \cdot \mathbf{u}^T)$.

Validation on analytical linear elasticity problem. The following experiment solves the static linear elasticity problem with homogeneous Dirichlet boundary conditions and a load applied inside the domain $\Omega = [0,1]^3$. The problem is borrowed from [24].

$$\nabla \cdot \sigma(\mathbf{u}) + \mathbf{f} = 0 \qquad \text{in} \quad \Omega$$
$$\sigma(\mathbf{u}) = \lambda(\nabla \cdot \mathbf{u})\mathcal{I} + \mu(\nabla \cdot \mathbf{u} + \nabla \cdot \mathbf{u}^T) \qquad \text{in} \quad \Omega \quad (11)$$
$$\mathbf{u} = 0 \qquad \text{on} \quad \partial\Omega$$

where the loading $\mathbf{f}$ and the Lamé parameters are detailed in [24]. The analytical expression of the displacement is

$$u_x = u_y = u_z = \sin(2\pi x)\sin(2\pi y)\sin(2\pi x)$$

The procedure for mesh generation is exactly the same as with the analytical Poisson problem experiment. Relative errors in L^2-norm are shown in figure 8. The conclusions drawn with the analytical Poisson problem apply here too: solutions computed with the hybrid space $\mathcal{H}yb_1, \mathcal{H}yb_{12}$ are close to the tri-linear ones ($\mathbb{Q}_1$) and significantly more accurate than solutions obtained with tetrahedra linear elements $\mathbb{P}_1$. On this specific example, the $\mathcal{H}yb_1$ solution is 3.5 times more accurate than the $\mathbb{P}_1$ one with the same number of degrees of freedom.

by the system:

$$\nabla \cdot \sigma(\mathbf{u}) + \mathbf{f} = 0 \qquad \text{in} \quad \Omega \qquad (6)$$
$$\sigma(\mathbf{u}) = \lambda(\nabla \cdot \mathbf{u})\mathcal{I} + \mu(\nabla \cdot \mathbf{u} + \nabla \cdot \mathbf{u}^T) \qquad \text{in} \quad \Omega \qquad (7)$$
$$\mathbf{u} = 0 \qquad \text{on} \quad \partial\Omega_D \qquad (8)$$
$$\sigma(\mathbf{u}) \cdot \mathbf{n} = g \qquad \text{on} \quad \partial\Omega_N \qquad (9)$$

where $\mathbf{n}$ is the exterior normal and $\mathcal{I}$ the identity matrix.

Weak formulation. For the weak formulation of the elasticity problem, we consider the simple displacement formulation (10). The derivation is similar to the Poisson problem but longer, the reader can refers to [20], [21] or

Simulations on more complex meshes. Besides the standard test cases, we applied our approach to hex-dominant meshes generated from industrial 3D models. The figure 9 illustrates a linear elasticity problem solved with $\mathcal{H}yb_1$ on a hexahedral-tetrahedra mesh generated with [6]. The 3D model *hanger* is borrowed from [25]. The solutions computed are consistent with the ones computed with standard Lagrange basis but further work is required to quantify precisely the differences. Indeed there are no analytical solution for non-trivial geometries and computing accurately a distance between finite element solutions defined on distinct meshes is not straightforward.

4. Conclusion

Two continuous function spaces, $\mathcal{H}yb_1$ and $\mathcal{H}yb_{12}$, defined on hybrid hexahedral-tetrahedral meshes have been introduced. The continuity of both the geometry and the function spaces is recovered using quadratic mappings and quadratic functions on tetrahedra connected to hexahedra, with constraints at hybrid junctions.

The experiments conducted on analytical problems with smooth solutions show that $\mathcal{H}yb_1, \mathcal{H}yb_{12}$ defined on hybrid meshes perform better (factor 3 in our tests) than $\mathbb{P}_1$ (tetrahedral meshes) and slightly worst than $\mathbb{Q}_1$ (hexahedral meshes). We conjecture with confidence that, under standard mesh shape and function regularity assumptions, $\mathcal{H}yb_1$ and $\mathcal{H}yb_{12}$ have a quadratic convergence rate in L^2-norm with mesh refinement and a linear convergence rate in H_1-norm.

Even if our current implementation works on any geometry, further research is required to quantify the errors obtained when applying the method on non-trivial geometries, especially the impact of hexahedral-tetrahedral meshes properties (proportion of tetrahedra, quality of elements). This requires techniques to compute distance between finite element solutions computed on distinct meshes. We are currently working on this topic.

Possible future work can be the extension of the proposed function spaces to higher orders by using standard Lagrange finite elements $\mathbb{Q}_k, \mathbb{P}_k$. For hexahedra $\mathbb{Q}_k$, functions restricted to faces are bi-variate polynomials of degree $2k$, so it should be possible to build *continuous* function spaces of order k with a mix of $\mathbb{Q}_k$ and $\mathbb{P}_{2k}$ finite elements subjected to appropriate constraints at hybrid interfaces.

Appendix A. Function basis of standard Lagrange finite elements

Appendix A.1. Reference tetrahedron and $\mathbb{P}_1, \mathbb{P}_2$ function spaces

The reference tetrahedron, denoted by $\hat{T}$, is defined by its 4 vertices $\hat{\mathbf{s}}_1 = (0,0,0)$, $\hat{\mathbf{s}}_2 = (1,0,0)$, $\hat{\mathbf{s}}_3 =$ $(0,1,0)$, $\hat{\mathbf{s}}_4 = (0,0,1)$. The barycentric coordinates of $\hat{T}$ are:

$$\hat{\lambda}_1(u,v,w) = 1 - u - v - w, \qquad \hat{\lambda}_2(u,v,w) = u$$
$$\hat{\lambda}_3(u,v,w) = v, \qquad \hat{\lambda}_4(u,v,w) = w$$

They satisfy $\forall i \in [1,4]$, $\lambda_i(\hat{\mathbf{s}}_j) = \delta_{ij}$, so they form a basis of the space of tri-variate polynomials of degree 1:

$$\mathbb{P}_1 = \{p(x,y,z) = ax + by + cz + d \text{ with } a,b,c,d \in \mathbb{R}\}$$

The decomposition on the basis is:

$$\forall p \in \mathbb{P}_1, \ p(u,v,w) = \sum_{i=1}^{4} p_i \ \hat{\lambda}_i(u,v,w) \ \text{ where } p_i = p(\hat{\mathbf{s}}_i)$$

The space of tri-variate polynomials of degree 2 is:

$$\mathbb{P}_2 = \{p(x,y,z) = \sum_{0 \leq i+j+k \leq 2} a_{ijk} x^i y^j z^k \text{ with } a_{ijk} \in \mathbb{R}\}$$

Its interpolating basis $(\hat{\phi}_i)_{i=1..10}$ can be expressed in terms of the barycentric coordinates:

$$\hat{\phi}_i(u,v,w) = \hat{\lambda}_i(2\hat{\lambda}_i - 1) \qquad 1 \leq i \leq 4$$
$$\hat{\phi}_{ij}(u,v,w) = 4\hat{\lambda}_i\hat{\lambda}_j \qquad 1 \leq i < j \leq 4$$

The first four functions are associated with the vertices $\hat{\mathbf{s}}_i$ of $\hat{T}$ and the last six functions are associated with the edge midpoints $\hat{\mathbf{s}}_{ij} = \frac{\hat{\mathbf{s}}_i + \hat{\mathbf{s}}_j}{2}$. The decomposition is:

$$\forall p \in \mathbb{P}_2, \ p(x,y,w) = \sum_{i=1}^{4} p_i\hat{\phi}_i(x,y,z) + \sum_{1 \leq i < j \leq 4} p_{ij}\hat{\phi}_{ij}(x,y,z)$$

where $p_i = p(\hat{\mathbf{s}}_i), p_{ij} = p(\hat{\mathbf{s}}_{ij})$

Proposition. *The restriction $p_{|t}$ of $p \in \mathbb{P}_2$ to a face $t \subset \hat{T}$ is a bi-variate polynomial of degree 2, which has 6 coefficients determined by the values of $p_{|t}$ at the 6 points $\hat{\mathbf{s}}_i, \hat{\mathbf{s}}_{ij} \in t$.*

Appendix A.2. Reference hexahedron and $\mathbb{Q}_1$ function space

In this work, the reference hexahedron $\hat{Q}$ is the unit cube $[0,1][0,1][0,1]$. The difference with the tetrahedron is that there are no barycentric coordinates but there is a symmetry of the cell along the three axis that we can exploit. We denote $(\hat{\mathbf{q}}_i)_{i=1..8}$ the vertices of $\hat{Q}$: $\hat{\mathbf{q}}_1 = (0,0,0)$, $\hat{\mathbf{q}}_2 = (1,0,0)$, $\hat{\mathbf{q}}_3 = (1,1,0)$, $\hat{\mathbf{q}}_4 = (0,1,0)$, etc.

By product of degree one polynomials $(x_i), (1 - x_i)$ defined along each axis, we can build the set $(\hat{\psi}_i)_{i=1..8}$ as follow:

$$\hat{\psi}_1 = (1-u)(1-v)(1-w) \qquad \hat{\psi}_5 = (1-u)(1-v)w$$
$$\hat{\psi}_2 = u(1-v)(1-w) \qquad \hat{\psi}_6 = u(1-v)w$$
$$\hat{\psi}_3 = uv(1-w) \qquad \hat{\psi}_7 = uvw$$
$$\hat{\psi}_4 = (u-1)v(1-w) \qquad \hat{\psi}_8 = (u-1)vw$$
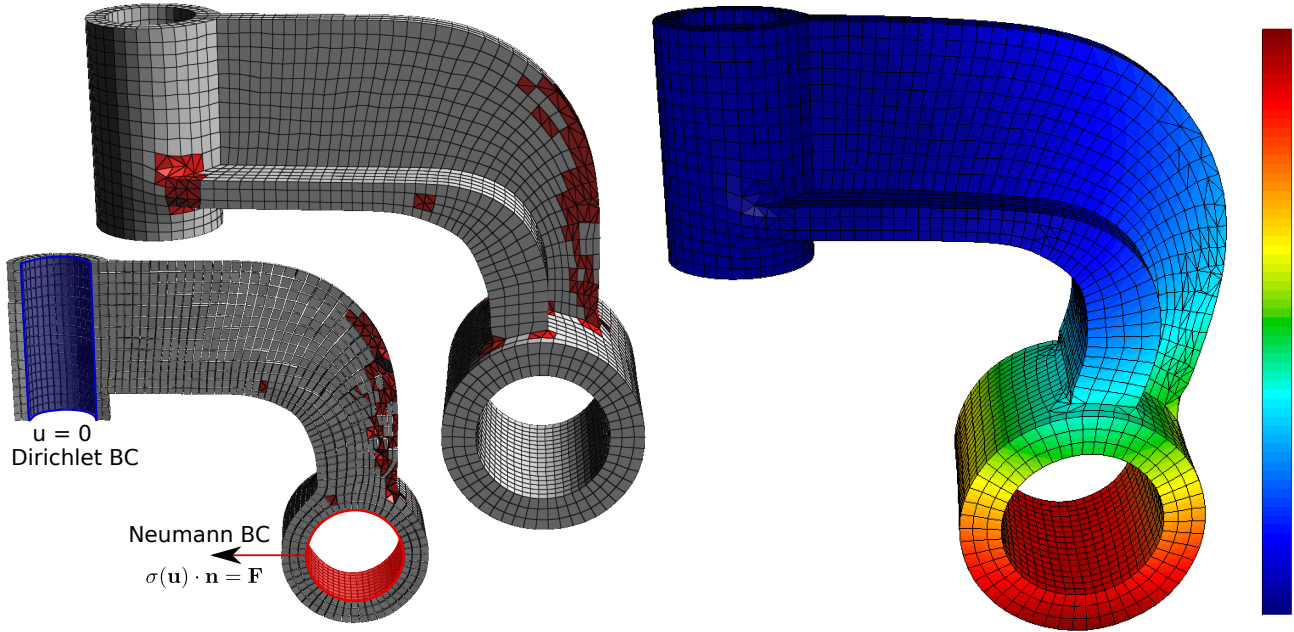
Figure 9: $\mathcal{H}yb_1$-finite element solution on hybrid hexahedral-tetrahedral mesh. On the left figure, tetrahedra are colored in red and hexahedra in grey. On the right figure, the color is the magnitude of the displacement field.

They satisfy $\hat{\psi}_i(\hat{\mathbf{q}}_j) = \delta_{ij}$, $1 \leq i, j \leq 8$ and form a basis of the space of tri-variate polynomials of degree one in each variable.

$$\mathbb{Q}_1 = \{p(x,y,z) = \sum_{0 \leq i,j,k \leq 1} a_{ijk} x^i y^j z^k \text{ with } a_{ijk} \in \mathbb{R}\}$$

We have the decomposition

$$\forall p \in \mathbb{Q}_1, \ p(x,y,w) = \sum_{i=1}^{8} p_i \hat{\psi}_i(x,y,z) \ \text{ where } p_i = p(\hat{\mathbf{q}}_i)$$

These polynomials are said to be tri-affine.

Proposition. *The restriction $p_{|q}$ of $p \in \mathbb{Q}_1$ to a face $q \subset \hat{Q}$ is a bi-variate polynomial of degree 1 in each variable, which has 4 coefficients determined by values of $p_{|q}$ at the 4 vertices of the face q.*

References

[1] P. Frey, P.-L. George, Mesh generation, Vol. 32, John Wiley & Sons, 2010.

[2] H. Si, Tetgen, a delaunay-based quality tetrahedral mesh generator, ACM Transactions on Mathematical Software (TOMS) 41 (2) (2015) 11.

[3] M. Staten, Why is hex meshing so hard? (2007).
URL www.scribd.com/doc/52824132/Why-Is-Hex-Meshing-So-Hard

[4] T. C. Baudouin, J.-F. Remacle, E. Marchandise, F. Henrotte, C. Geuzaine, A frontal approach to hex-dominant mesh generation, Advanced Modeling and Simulation in Engineering Sciences 1 (1) (2014) 1–30.

[5] A. Botella, B. Lévy, G. Caumon, Indirect unstructured hex-dominant mesh generation using tetrahedra recombination, Computational Geosciences (2015) 1–15.

[6] D. Sokolov, N. Ray, L. Untereiner, B. Lévy, Hexahedral-dominant meshing.
URL https://hal.inria.fr/hal-01203544

[7] P.-E. Bernard, J.-F. Remacle, N. Kowalski, C. Geuzaine, Frame field smoothness-based approach for hex-dominant meshing, Computer-Aided Design 72 (2016) 78–86.

[8] J. Chan, Z. Wang, A. Modave, J.-F. Remacle, T. Warburton, Gpu-accelerated discontinuous galerkin methods on hybrid meshes, arXiv preprint arXiv:1507.02557.

[9] M. Bergot, M. Duruflé, Higher-order discontinuous galerkin method for pyramidal elements using orthogonal bases, Numerical Methods for Partial Differential Equations 29 (1) (2013) 144–169.

[10] S. J. Sherwin, T. C. Warburton, G. E. Karniadakis, Spectral/hp methods for elliptic problems on hybrid grids, Contemporary Mathematics 218 (1998) 191–216.

[11] M. Bergot, G. Cohen, M. Duruflé, Higher-order finite elements for hybrid meshes using new nodal pyramidal elements, Journal of Scientific Computing 42 (3) (2010) 345–381, cool 3D experiments.

[12] G. Bedrosian, Shape functions and integration formulas for three-dimensional finite element analysis, International journal for numerical methods in engineering 35 (1) (1992) 95–108.

[13] C. Durochat, S. Lanteri, C. Scheid, High order non-conforming multi-element discontinuous galerkin method for time domain electromagnetics, Applied Mathematics and Computation 224 (2013) 681–704.

[14] R. Léger, J. Viquerat, C. Durochat, C. Scheid, S. Lanteri, A parallel non-conforming multi-element dgtd method for the simulation of electromagnetic wave interaction with metallic nanoparticles, Journal of Computational and Applied Mathematics 270 (2014) 330–342.

[15] H. Fahs, High-order discontinuous galerkin method for time-domain electromagnetics on non-conforming hybrid meshes, Mathematics and Computers in Simulation 107 (2015) 134–156.

[16] N. Marais, D. B. Davidson, Conforming arbitrary order hexahedral/tetrahedral hybrid discretisation, Electronics Letters 44 (24) (2008) 1384–1385.

[17] D. L. Dewhirst, P. M. Grinsell, Joining tetrahedra to hexahedra, in: MSC 1993 World Users, 1993.

[18] S. J. Owen, S. A. Canann, S. Saigal, Pyramid elements for maintaining tetrahedra to hexahedra conformability.

[19] P. George, H. Borouchaki, Construction of tetrahedral meshes of degree two, International Journal for Numerical Methods in Engineering 90 (9) (2012) 1156–1182.

[20] P. G. Ciarlet, The finite element method for elliptic problems, North-Holland, 1978.

[21] A. Ern, J.-L. Guermond, Theory and practice of finite elements, Springer, 2004.

[22] A. Gregoire, A. Craig, Numerical analysis and optimization: an introduction to mathematical modelling and numerical simulation, 2007.

[23] Mfem: Modular finite element methods, `mfem.org`.

[24] D. Schillinger, J. A. Evans, F. Frischmann, R. R. Hiemstra, M.-C. Hsu, T. J. Hughes, A collocated c0 finite element method: Reduced quadrature perspective, cost comparison with standard finite elements, and explicit structural dynamics, International Journal for Numerical Methods in Engineering 102 (3-4) (2015) 576–631.

[25] M. Livesu, A. Sheffer, N. Vining, M. Tarini, Practical hex-mesh optimization via edge-cone rectification, ACM Transactions on Graphics (TOG) 34 (4) (2015) 141.